Fuel Processing Technology 254 (2024) 108032

Contents lists available at ScienceDirect

Fuel Processing Technology

journal homepage: www.elsevier.com/locate/fuproc

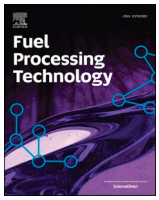

Research article

Simulation of a sorption-enhanced water gas-shift pilot technology for pure hydrogen production from a waste gasification plant

Barbara Malsegna [a,b], Alex Sebastiani [b], João Guilherme da Gama Paz-Dias [b], Francesco Di Luca [c], Andrea Di Giuliano [a], Katia Gallucci [a], Massimiliano Materazzi [b,*]

[a] University of L'Aquila, Department of Industrial and Information Engineering and Economics (DIIIE), Piazzale E.Pontieri 1-loc. Monteluco di Roio, 67100 L'Aquila, Italy
[b] University College London, Department of Chemical Engineering, London WC1E7JE, UK
[c] ITALFLUID COSMEP srl, Via Vivaldi 4, Montesilvano 65015, Pescara, Italy

ARTICLE INFO

Keywords:
Sorption-enhanced water-gas shift
Hydrotalcite
Waste gasification
Renewable hydrogen
BECCS

ABSTRACT

This study has analysed and optimised a 5-column sorption enhanced water gas shift (SEWGS) pilot unit, set to operate for the first time in a waste gasification facility for the production of transport-grade hydrogen and CO_2 streams. Full process simulation was undertaken by developing a one-dimensional model of each reactor, with boundary conditions directly informed by real plant operation. From the sensitivity analysis performed, syngas flowrate variations were seen to have a minor but temporary, impact on hydrogen product specifications, while changes to syngas composition were shown to have a longer-lasting effect on system performance. Based on full cycle operation results, the current 5-column SEWGS unit design was concluded to be inadequate for fuel-cell-grade H_2 production, despite obtaining a high H_2 purity of 99.5%, mainly due to its excessive steam consumption. However, the process achieved an exceptionally high CO_2 purity of 99.9%, and 88.6% hydrogen recovery rate, suggesting its potential use in carbon capture and heat-grade hydrogen production applications.

1. Introduction

In 2022 the International Energy Agency (IEA) reported that around 80% of global energy is provided by fossil fuels [1]. Reducing and mitigating the associated CO_2 emissions has become a significant climate challenge, requiring the transition to renewable energy systems as the primary objective of most countries' net-zero agenda. Hydrogen represents a promising solution as a clean energy carrier and storage, as well as for its zero end-use emissions [2]. However, natural gas reforming is still the predominant industrial process for generating hydrogen resulting in substantial CO_2 emissions due to the fossil nature of the feedstock [3]. Carbon Capture and Storage (CCS) technology integrated into gas reforming is considered the most practical solution to reduce emissions for hydrogen production in the short to mid-term [4]. However, CCS's current cost and efficiency limitations need to be addressed to compete with other emerging technologies in the longer term [5,6]. Carbon capture and reduction (CCR) technology is a possible different route that has gained interest to directly convert CO_2 to value-added products [7]. As to hydrogen production, water electrolysis is being explored and promoted as an alternative; however, the climate benefits of H_2 from water splitting would only be real if the electricity is supplied solely by renewable energy sources, which are often discontinuous, unpredictable, and geographically constrained [8].

Biomass holds great potential as a renewable feedstock for energy, fuels, and chemical production (e.g., hydrogen), via thermochemical conversion like pyrolysis or gasification [9,10]. Biomass and biowaste offer the advantage of being carbon neutral and, combined with CCS in what is defined as Bioenergy with Carbon Capture and Storage (BECCS), could further enhance climate performance as a carbon-negative technology [9,11,12].

In the production of hydrogen from biomass, also referred to as biohydrogen, the choice of feedstock is crucial as it significantly influences the performances of the process, in particular the processing and purification steps required. Hydrogen derived from organic or partially organic waste is particularly interesting as it offers a solution to both waste disposal issues and the cost/availability of the feedstock [13]. The IEA emphasizes the significant potential of biohydrogen in reducing greenhouse gas (GHG) emissions and highlights the growing interest in producing hydrogen from renewable sources [14–16].

The overall process considered in this work is the production of

* Corresponding author.
E-mail address: massimiliano.materazzi.09@ucl.ac.uk (M. Materazzi).

https://doi.org/10.1016/j.fuproc.2024.108032
Received 24 October 2023; Received in revised form 3 January 2024; Accepted 3 January 2024
Available online 11 January 2024

hydrogen from the gasification of refuse-derived fuel (RDF) generated from biomass-rich (>60% wt.) household waste. The suitability of producing low-carbon hydrogen from the gasification of waste feedstock has already been proven at a pilot and demonstration scale in previous work by Materazzi et al. [17]. Although the hydrogen synthesis process offers numerous environmental benefits, the costs associated with gas cleaning and carbon capture plants might hinder its commercial potential [18]. Compared to more conventional fossil based feedstock, biomass and waste biomass contain much higher quantities of oxygen, which reflect to higher steam and CO2 concentration in the syngas (this is especially true in autothermal gasifiers). This factor, together with the varying C:H ratio and potential fluctuations in gas composition due to heterogeneity of waste, make the product syngas quite distinct from other applications, and introduce different challenges in the carbon capture systems. In this respect, one of the main challenges lies in the operational cost of regenerating solvents used in gas separation methods, either physical or chemical based. Furthermore, it should be noted that although CO_2 absorption using liquid solvents is the most mature and commercially available technology for separating CO_2, the high energy consumption during solvent regeneration and potential solvent degradation could lead to process inefficiencies, solvent loss and toxic byproducts [19,20]. To make the process economically attractive at a low scale, more typical of BECCS, it is essential to reduce capital costs by improving compactness and efficiency. Process Intensification is a chemical engineering concept based on improving the performance of the overall process [21]. In this context, Sorption-Enhanced Water-Gas Shift (SEWGS) emerges as a promising pre-combustion carbon capture technology. SEWGS combines the Water Gas Shift reaction (WGS) (Eq. (1)) with in situ adsorption of CO_2 (Eq. (2)), maximizing hydrogen production from syngas while simultaneously capturing and separating CO_2 in a single-unit operation [21–23]. This intensified process utilizes Pressure Swing Adsorption (PSA), employing solid material for reversible CO_2 adsorption at temperatures ranging from 300 to 500 °C and pressure around 20–40 bar [24].

$$CO + H_2O \rightleftharpoons CO_2 + H_2 \quad \Delta H^0_{298\ K} = -41\ kJ\ mol^{-1} \tag{1}$$

$$CO_2 + ads \rightleftharpoons CO_2 - ads \tag{2}$$

Compared to conventional processes, SEWGS offers the advantage of reduced process steps and required equipment [24,25]. The benefits of SEWGS have been extensively studied and experimentally demonstrated [24,26–29]. Hydrotalcite-based materials, and in particular potassium-promoted-hydrotalcite (K-HTC), have been the most used in SEWGS processes [30–32], due to their chemical robustness, partial catalytic activity for the WGS reaction, ability to co-capture other acid gas components with CO_2, fast sorption kinetics, stable cyclic performances, and efficient regeneration through pressure swing [28,33,34]. This enables the SEWGS process to obtain a high carbon capture rate and CO_2 purities in the carbon dioxide effluent stream, making it ideal for CCS applications [35–37]. TNO research groups extensively studied the SEWGS technology in an Integrated Gasification Combined Cycle (IGCC) power plant for H_2 production and in integrated steelwork for H_2 production and simultaneous carbon capture. However, no previous studies have explored the potential of applying SEWGS in a waste gasification plant, and only a few literature papers have focused on the effects of SEWGS operational parameters on hydrogen purity (HP) and hydrogen recovery ratio (HRR) due to the emphasis on carbon capture over hydrogen production [38].

This work aims to assess the suitability of a simplified SEWGS system to generate fuel-cell grade hydrogen (HP > 99.97%) from waste-derived syngas at low pressure (typical of gasification plants), as well as a CO_2 stream suitable for storage (purity >95%). To this end, a numerical simulation was developed to explore the integration possibilities of a novel 5-column pilot scale SEWGS unit into an existing waste gasification plant, and to determine the optimal operating conditions and parameters for the SEWGS pilot unit design. The efficiency of the process was assessed by analysing the recovery rates of each product, along with the overall steam consumption, which affects the operational costs and the environmental impact of the process. The optimal configuration and design parameters are evaluated, such as the time step duration, rinse configuration (co-current or counter-current) and steam demand for the SEWGS process to achieve the required process specifications. Additionally, variations in syngas feed flowrate and composition during the adsorption step were explored to understand the SEWGS process's sensitivity to common disturbances in bioenergy plants when operated on waste feedstock, which has high variability in density and composition due to its heterogeneous nature. Accomplishing these objectives is deemed important for understanding the operational performance of the low-pressure SEWGS process applied specifically to BECCS for high-purity hydrogen production, which is a novel concept from an industrial and literature standpoint.

2. Material and methods

2.1. Plant description

This work focused on the integration of SEWGS into an already existing demonstration scale (4.4 MW_{th} input) waste gasification plant operated in Swindon UK, originally designed to produce either pure H_2 or bioSNG and CO_2 within the *Hydrogen Greenhouse Gas Removal (GGR) Demonstration project* [39].

The gasification plant treats approximately 850 kg/h of RDF or waste wood into a two-stage thermochemical process for the conversion of the solid feedstock into clean syngas. The composition of the fed RDF investigated in this work is summarized in Table 1. The two-stage process consists of a steam-oxygen gasifier for syngas generation and a plasma reactor for tar reforming. The stream is then passed into a cleaning section using conventional technologies, e.g., dry filters, a combination of acid and alkaline scrubbers, and ZnO guard beds. In its original configuration, the hydrogen fraction of the clean syngas is increased via a series of catalytic high and low-temperature water gas shift reactors (HTS and LTS). The H_2-rich stream is polished of CO traces through a methanation step (MTH), followed by a separation stage where CO_2 is chemically adsorbed, separated and made ready for transportation and storage [4]. The hydrogen stream is further purified in a PSA to achieve fuel-cell grade purity levels. This study focuses on a 50 kg/h slipstream of syngas, which is diverted from the plant after the high-temperature WGS to the new SEWGS facility for pure H_2 and CO_2 production. A flow diagram of the demonstration plant is reported in Fig. 1, together with the pilot SWGS unit studied in this work.

The feedstock characterization and the syngas composition at different stages of the process (namely, the clean syngas before HTS and the shifted gas after HTS) are reported in Table 1. RDF data are reported for the baseline case, and possible variations are registered during plant operation. This variation would be reflected in gas composition and flowrate ranges, with oscillations typically in the range of +/− 5%. Lower oscillations are instead reported for syngas post-HTS, due to the buffering effect of the water gas shift step, and the higher dilution in steam.

The SEWGS pilot unit under investigation is composed of five reactors (Fig. 2), each with a height of 2.5 m and an internal diameter of 0.23 m. This configuration and number of columns, although sub-optimal, were first selected to assess the potential for a continuous generation of hydrogen and carbon dioxide product stream under PSA operation. The reactor design parameters are also shown in Fig. 2.

2.2. Mathematical model description

A dynamic one-dimensional isothermal model for an axially dispersed plug flow SEWGS reactor has been developed. The cylindrical reactor is assumed to be packed with a mixture of catalyst and sorbent particles (adsorbent/catalyst volume ratio of 5): (i) a commercial

Table 1
RDF and Syngas specifications.

Proximate analysis [wt% dry ash free (DAF)]	Typical Value	Lower Limit	Maximum Limit	Cleaned Syngas Composition (mol%)		Syngas post-HTS Avg. Composition (mol%)	
Fixed Carbon	8.90	5.5	10.5	H_2	34.7 (± 5%)	H_2	29.5 (± 2.5%)
Volatile matter	64.7	60.2	70.5	CO	42.6 (±5%)	CO	2.30 (± 2.5%)
Ash	11.8	5.0	19.5	CO_2	12.2 (± 5%)	CO_2	20.0 (± 2.5%)
Moisture	14.6	6.0	16.6	CH_4	0.1	CH_4	0.0
Ultimate Analysis [wt% DAF]	Typical Value	Lower Limit	Maximum Limit	H_2O	10.1	H_2O	47.9
Fossil C	20.51	20.0	30.0	N_2	0.30	N_2	0.30
Biogenic C	36.23	30.0	40.0				
H	6.86	4.5	7.0				
O	31.78	25.6	35.0				
N	4.1	1.5	8.5				
S	0.18	0.1	0.3				
Cl	0.34	0.1	0.4				

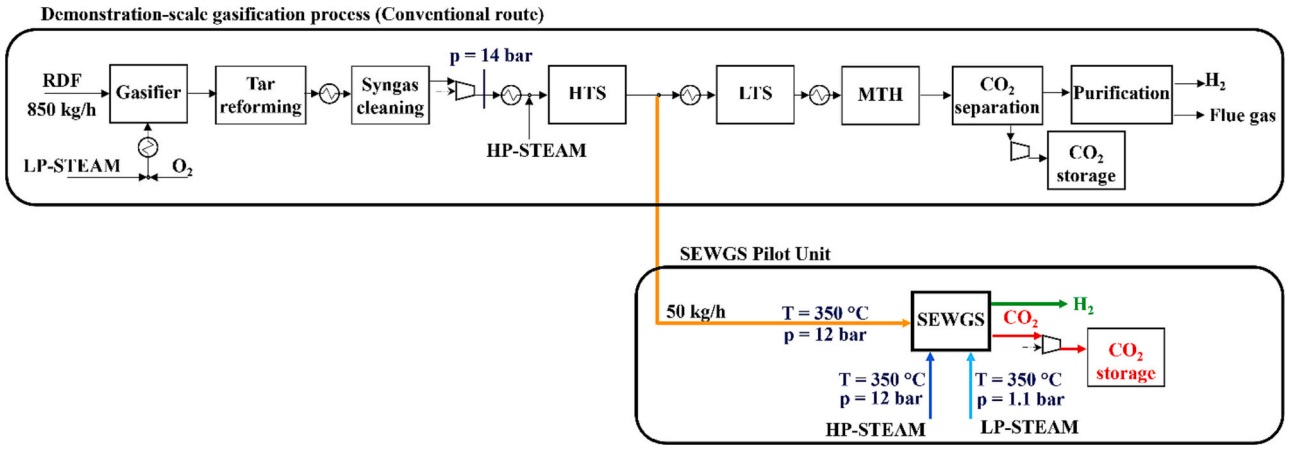

Fig. 1. Flow diagram for a demonstration plant for H_2 production and newly developed pilot for SEWGS.

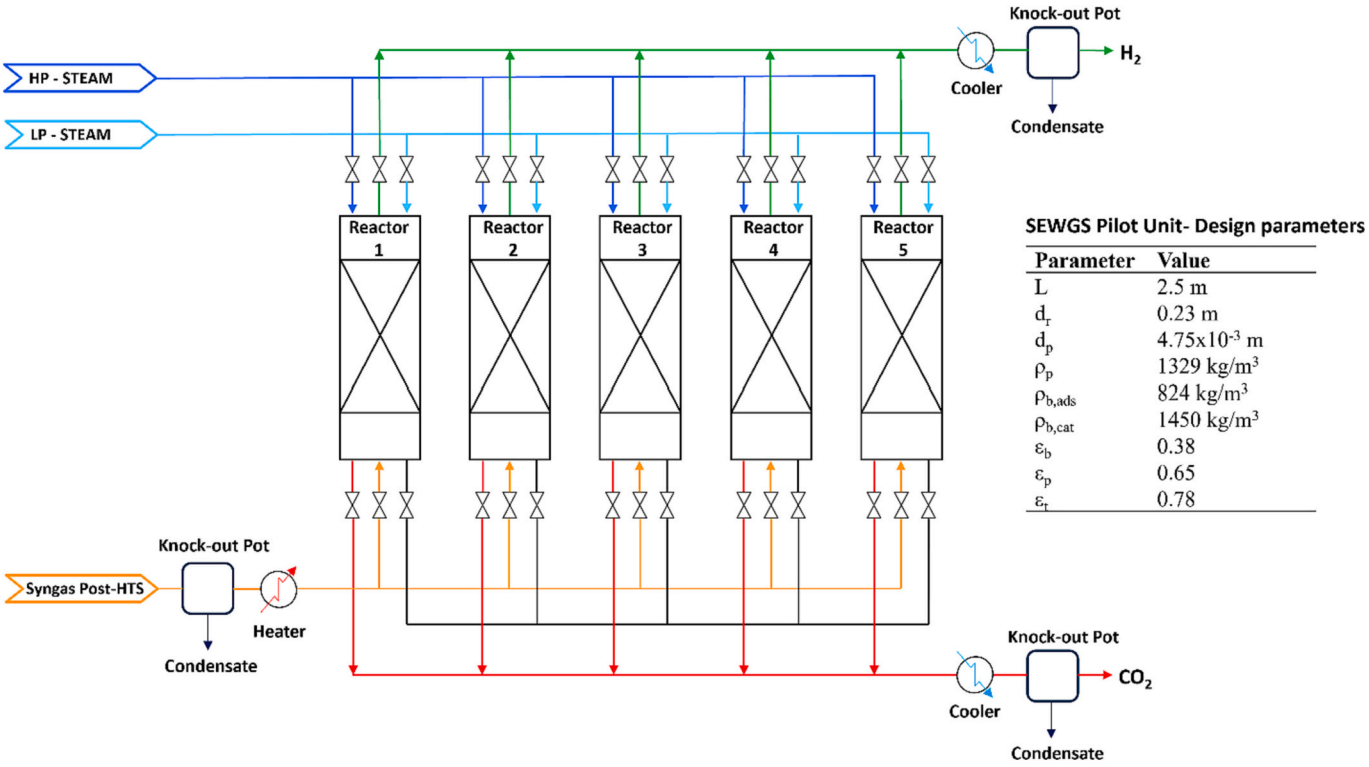

Fig. 2. Configuration and design parameter of the SEWGS pilot unit.

Table 2
Reactors governing equation.

Component mass balance $\varepsilon_t \frac{\partial c_{CO_2}}{\partial t} = -\frac{\partial (u c_{CO_2})}{\partial z} + \frac{\partial}{\partial z}\left(cD_{ax}\frac{\partial y_{CO_2}}{\partial z}\right) + \rho_{b,cat} r_{WGS} - \rho_{b,ads}\frac{\partial q_{CO_2}}{\partial t}$	Eq. 3	Ref. [40,47,48]
$\varepsilon_t \frac{\partial c_i}{\partial t} = -\frac{\partial u c_i}{\partial z} + \frac{\partial}{\partial z}\left(cD_{ax}\frac{\partial y_i}{\partial z}\right) + \rho_{b,cat} r_{WGS}\ i = H_2, CO, H_2O, N_2$.	Eq. 4	
Overall mass balance $\varepsilon_t \frac{\partial c}{\partial t} = -\frac{\partial (uc)}{\partial z} + \rho_{b,cat} r_{WGS} - \rho_{b,ads}\frac{\partial q_{CO_2}}{\partial t}$	Eq. 5	Ref. [47]
Equation of State $pM_{av} = \rho_g RT$	Eq. 6	
Momentum balance $\frac{\partial p}{\partial z} = -K_D u - K_V u^2$	Eq. 7	Ref. [49]
CO_2 adsorption kinetic $\frac{\partial q_{CO_2}}{\partial t} = k_{LDF,CO_2}\left(q^{eq}_{CO_2} - q_{CO_2}\right)$	Eq. 8	Ref. [24,41]:

Table 3
Parameters of governing equations.

Parameters of the Momentum balance (Ergun equation) $K_D = \frac{150\mu(1-\varepsilon_b)^2}{d_p^2 \varepsilon_b^3}; K_V = \frac{1.75(1-\varepsilon_b)\rho_g}{d_p \varepsilon_b^3}$	Ref. [49,50]
Axial Dispersion coefficient D_{ax} $D_{ax} = 0.73D_m + \frac{0.5 u d_p}{1 + 9.49\frac{D_m}{u d_p}}$ with: $D_{m,i} = \sum_{i=1}^{n} D_{m,i} y_i$	Ref. [21,48]
Modified Langmuir Isotherm $q^{eq}_{CO_2} = \frac{q^s_{CO_2} K_{CO_2} p_{CO_2}}{1 + K_{CO_2} p_{CO_2}} + \frac{A_{CO_2} V_0}{v_{m,CO_2}}$ with $A_{CO_2} = exp\left(-\left[\left(\frac{RT}{E_i}\right) ln\left(\frac{p_{0,i}}{p_i}\right)\right]^{m_i}\right), p_{0,CO_2} = p_{c,CO_2}\left(\frac{T}{T_{c,CO_2}}\right)^2, v_{m,CO_2} = \frac{RT_{c,CO_2}}{8p_{c,CO_2}}$ in which: $q^s_{CO_2} = 0.45\ mol \bullet kg^{-1}$ $\quad K_{CO_2} = 28\ MPa^{-1}$ $E_{CO_2} = 23\ kJ \bullet mol^{-1}$ $\quad m_{CO_2} = 5.2$ $V_0 = 74\ cm^3 \bullet kg^{-1}$	Ref. [24,26]
Mass-transfer coefficient $k_{LDF,CO_2} = \frac{15}{r_p^2}\frac{\varepsilon_p D_p}{\varepsilon_p + \rho_p RT\left(\frac{\partial q^{eq}_{CO_2}}{\partial p_{CO_2}}\right)}$ in which $D_p = 3.3 \times 10^{-7} m^2 \bullet s^{-2}$	Ref. [24,48,51]
WGS reaction rate expression $r_{WGS} = kp_{CO}p_{H_2O}\left(1 - \frac{p_{H_2}p_{CO_2}}{p_{CO}p_{H_2O}}\frac{1}{K_{eq}}\right)$ with: $k = 8.689 \times 10^{-7} exp\left(-\frac{32.839}{RT}\right)$ $K_{eq} = exp\left(-0.29353Z^3 + 0.63508Z^2 + 4.1778Z + 0.31688\right)$ with: $Z = \frac{1000}{T} - 1$ physical properties of gaseous species were calculated using Aspe Plus V11	Ref. [52,53]

iron-chromium-based material was assumed as the high-temperature WGS catalyst and (ii) K-HTC as the CO_2 sorbent.

Other groups have used a similar modelling approach for sorption-enhanced processes by packed-bed reactors [24,40–44]. The main assumptions used to develop the model are given below:

- The reactor is a tubular, packed-bed reactor, operated dynamically and isothermally.
- The flow pattern can be described by an axially dispersed plug flow model.
- The model is one-dimensional, so the radial gradients of the concentrations, adsorbent loading, fluid velocity, and pressure are not taken into account.
- The mass transfer between gas and solid is sufficiently fast, making interparticle gradients of concentrations and temperature negligible.
- All gaseous components are considered ideal gases.

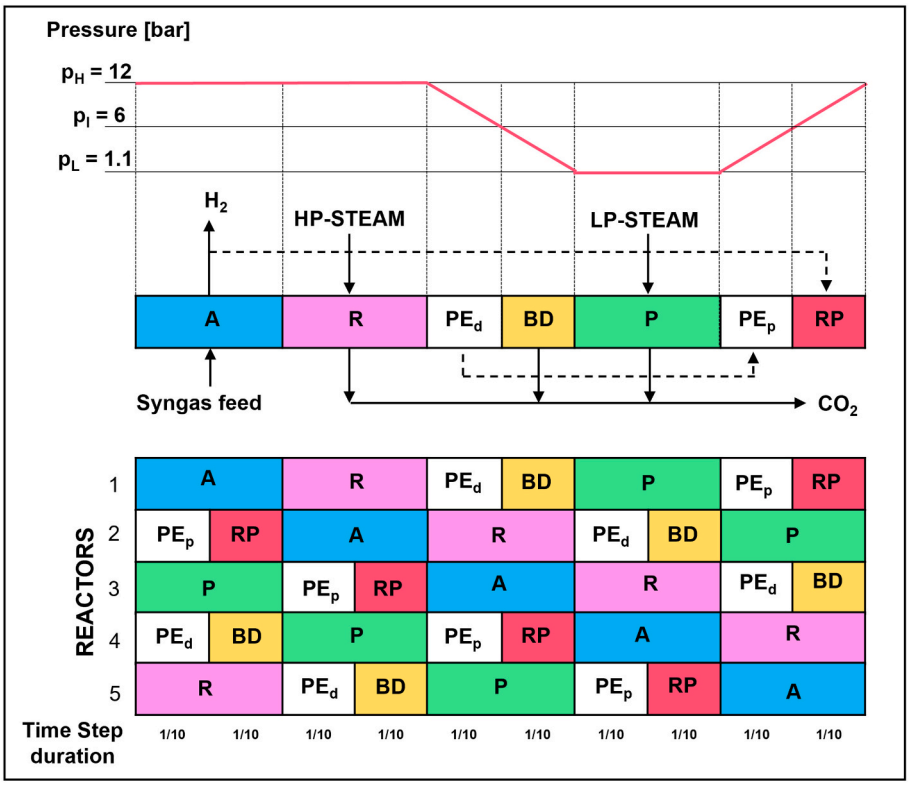

Fig. 3. Base case operating schedule of SEWGS pilot unit (A: adsorption, R: rinse, PE_d: pressure equalization depressurization, BD: blow down, P: purge, PE_p: pressure equalization pressurization, RP: repressurization).

- The WGS reaction is the only one taking place in the reactor.
- An effectiveness factor of unity is assumed for the catalyst particles, i.e., intraparticle diffusion limitations are negligible, in line with similar studies [46–49]
- Sorbent is assumed to exhibit no catalytic properties towards the WGS reaction and carbon dioxide is the only adsorbed species (i.e., water adsorption on the K-HTC sorbent was neglected) [41].
- The Linear Driving Force (LDF) approximation is used to describe the kinetic of carbon dioxide between the gaseous and sorbent phases.
- A modified Langmuir isotherm is used to describe the equilibrium adsorption of carbon dioxide on the sorbent [26].

Based on these assumptions, the governing equations that model each reactor vessel were obtained. Table 2 shows those governing equations, while the related parameters are calculated as summarized in Table 3. The model, and its assumptions on sorbent catalyst therein, was validated through dedicated adsorption tests on a single tube, lab scale apparatus, as reported in Supplementary Material. It is important to emphasise that the value chosen for the maximum sorption capacity is very conservative (q^s_{CO2} = 0.45 mol·kg^{-1}, Table 3) compared to those reported elsewhere [45,46]. This was assumed on the basis that partial deactivation of the sorbent could take place at full regime, upon exposure to trace (undetected) contaminants in a waste gasification plant.

2.3. SEWGS cycle process description and modelling approach

The process illustrated in Fig. 2 follows the typical approach of a pressure swing multicomponent system. In particular, the whole SEWGS cycle for CO_2 capture consists of seven distinct steps, performed in sequence by each reactor, as schematized in Fig. 3. The cycle steps include (Fig. 3): adsorption (A), rinse (R), pressure equalization - depressurization (PE_d), blow down (BD), purge (P), pressure equalization - pressurization (PE_p), and repressurization (RP). In each step of Fig. 3, details of co-current and counter-current flow pattern are also shown. The adsorption step (A) is the only stage that generates H_2 product with this configuration, while the counter-current rinse step (R), the blow down step (BD), and the purge step (P) all contribute to the CO_2 product stream. The operating temperature is set to be 350 °C at all steps. The maximum operating pressure of the SEWGS unit is 12 bar (p_H) during adsorption and rinse step and the minimum is 1.1 bar (p_L) in purge step, with an intermediate pressure of 6 bar (p_I) at the end of the pressure equalization steps. Operating pressure was intentionally selected to be relatively low to facilitate plant integration and material selection. This is a novel process choice, as a typical PSA system would work at much higher inlet pressure. As for the stream available in this process, these comprise of a post-HTS clean syngas feed stream, along with high-pressure and low-pressure steam utility streams (HP-STEAM and LP-STEAM, respectively), and a hydrogen repressurization stream (see Fig. 2). The syngas stream is fed at a flowrate of 50 kg/h to the adsorption step and is assumed to be free of contaminants (sulphur, nitrogen-, and chlorine-based compounds, alkali metals, ash, etc.), as the stream has undergone extensive gas cleaning process before entering in the SEWGS section. The steam utility stream consists of pure water vapour at a pressure of 12 bar for the HP-STEAM and 1.1 bar for the LP-STEAM, both fed at 350 °C. The hydrogen repressurization stream is used to bring the last step (RP) column to its original pressure and is assumed to be composed of pure hydrogen gas at 350 °C and 12 bar. The governing equations (Eqs. (3)–(8), Table 2) for modelling a single bed were extended to simulate the SEWGS cyclic process by selecting appropriate initial and boundary conditions [41]. The model considers multicomponent mass balance (Eqs. (3)–(4), Table 2), overall mass balance (Eq. (5), Table 2), Ergun relation for pressure drops (Momentum balance, Eq. (7), Table 2), and nonlinear adsorption equilibrium isotherm (Table 3) coupled with WGS reaction (Table 3), resulting in a system of Partial Differential Equations (PDEs). The variables that can be calculated at each cyclic process step include gas-phase component molar fraction (y_{CO_2}, y_{CO}, y_{H_2}, y_{H_2O}, y_{N_2}), CO_2 captured by the sorbent ("CO_2 loading", q), gas superficial velocity (u) and pressure (p). The

Method-of-Line [23,54] is used to solve the PDEs system by initially approximating spatial derivatives with algebraic equations, which are then transformed into a set of Ordinary Differential Equations (ODEs), solvable by dedicated numerical methods. Spatial discretization is achieved using a uniform grid and finite difference technique in the axial direction (z, Table 2). The resulting ODEs system is solved numerically with respect to time (t, Table 2) using MATLAB "ode15s" solver. Fig. 3 depicts the cycle timing for five parallel reactors, which is controlled by setting the total cycle time and dividing it into steps based on the specified time step duration. A 1/10-time step duration of 90 s is used as the first attempt value.

Simulations were performed using a single bed approach, i.e., following the evolution of all consecutive steps of the SEWGS cycle (as given in Fig. 3), as experienced by one of the five reactors. At the end of each step, the final gas composition expressed as molar fraction, pressure, gas superficial velocity, and (residual) CO_2 loading on the sorbent were saved and used as the initial conditions of the following step in the SEWGS cycle sequence. In the first step, the column was initially purged with pure nitrogen gas at 12 bar and 350 °C.

2.4. Performance analysis

This study aimed to analyse the SEWGS system's operation and determine its viability in generating high purity hydrogen, in order to understand its potential applications, such as the production of fuel-cell-grade hydrogen or CCS-grade carbon dioxide. A parametric analysis was carried out, considering three main operating parameters: time step duration, steam flowrate in the rinse step (R, Fig. 3), and steam flowrate in the purge step (P, Fig. 3). Strict requirements exist for polymeric fuel-cell-grade hydrogen regarding CO and CO_2 levels, which must be below 0.2 μmol/mol and 2 μmol/mol, respectively [55,56]. The time step duration in the SEWGS process can be evaluated during the adsorption step, to ensure that product hydrogen met those requirements. However, certain steps may need longer duration than allowed in the scheduled cyclic process, disrupting the continuity and preventing a continuous flow product, so an optimization exercise is often needed. The steam flowrate in the rinse and purge steps is analysed independently to ensure optimal H_2 and CO_2 purities in the respective product stream. The rinse and purge steam flowrates are determined by the rinse-to-carbon (R/C, Eq. (9)) and purge-to-carbon (P/C, Eq. (10)) ratios.

$$R/C = \frac{\int_0^{t_R} F_{Steam,R}\,dt}{\left(y_{CO,Feed} + y_{CO_2,Feed}\right) F_{Feed} t_A} \tag{9}$$

$$P/C = \frac{\int_0^{t_P} F_{Steam,P}\,dt}{\left(y_{CO,Feed} + y_{CO_2,Feed}\right) F_{Feed} t_A} \tag{10}$$

The steam flowrate in these steps influences several efficiency aspects of the SEWGS process, as it impacts the recovery of H_2 and CO_2, as well as the economic and environmental aspects related to energy and emissions for steam generation. To objectively evaluate the parameter influences, key performance indicators (KPIs) were defined for the SEWGS pilot unit (Table 4) on integral base with respect to time: hydrogen recovery ratio (HRR, Eq. (11)), carbon capture ratio (CCR, Eq. (12)), carbon purity (CP, Eq. (14)), and hydrogen purity (HP, Eq. (13)). In Eqs. (11)–(14), the letter j denotes steps contributing to the hydrogen product stream (j = A, Eq. (11), Eq. (13)), while k denotes the steps contributing to the carbon dioxide product stream (k = R/BD/P, Eq. (12), Eq. (14)). It is important to note that the purities of H_2 and CO_2 in their respective product stream were determined on a dry basis.

3. Results and discussion

3.1. Adsorption step

The optimal time intervals for the SEWGS model were assessed considering the restrictions on CO and CO_2 content in the hydrogen product stream for transport applications. The amounts of CO_2 and CO leaving the adsorption step were calculated every 30 s (in micromoles of CO_2 or CO per total moles of dry hydrogen product, i.e., μmol/mol), as shown in Fig. 4a-b.

As the adsorption time increases, more reactants are fed to the column, involving a growing amount of sorbent particles into CO_2 capture. This, in turn, reduces the overall sorption capacity of the bed and increases the concentration of CO_2 along the column. As a results, the rate of the forward WGS reaction decreases, causing a decrease in the conversion of CO and a significant rise in the CO impurities content in the hydrogen product. Fig. 5 show a clear advancement of the adsorption front with longer step duration. As the sorbent progressively becomes

Table 4
Description of the KPIs used in this work.

KPI	Definition	Formula	
HRR [%]	Ratio of actual H_2 product recovered to maximum obtainable H_2	$HRR = \frac{\sum_j \int_0^{t_j} y_{H_2,out,j}\, F_{out,j}\,dt}{\left(y_{H_2,Feed} + y_{CO,Feed}\right) F_{Feed} t_A} \times 100$	Eq. 11
CCR [%]	Ratio of actual CO_2 product recovered to maximum obtainable CO_2	$CCR = \frac{\sum_k \int_0^{t_k} y_{CO_2,out,k}\, F_{out,k}\,dt}{\left(y_{CO_2,Feed} + y_{CO,Feed}\right) F_{Feed} t_A} \times 100$	Eq. 12
HP [%]	Dry-basis H_2 product purity	$HP = \frac{\sum_j \int_0^{t_j} y_{H_2,out,j}\, F_{out,j}\,dt}{\sum_j \int_0^{t_j} F_{out,j}\,dt - \sum_j \int_0^{t_j} y_{H_2O,out,j} F_{out,j}\,dt} \times 100$	Eq. 13
CP [%]	Dry-basis CO_2 product purity	$CP = \frac{\sum_k \int_0^{t_k} y_{CO_2,out,k}\, F_{out,k}\,dt}{\sum_k \int_0^{t_k} F_{out,k}\,dt - \sum_k \int_0^{t_k} y_{H_2O,out,k}\, F_{out,k}\,dt} \times 100$	Eq. 14

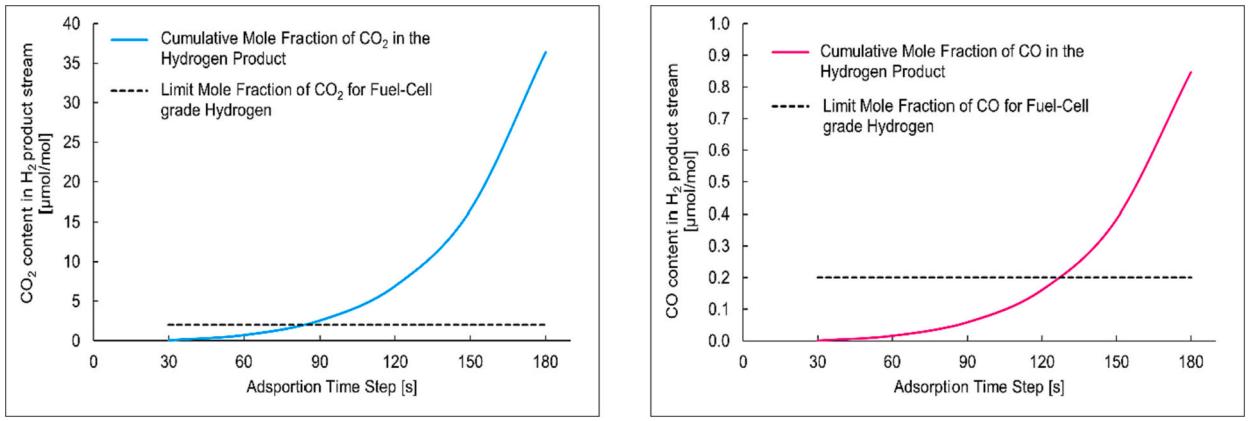

Fig. 4. a) CO_2 content in the outlet hydrogen product stream as a function of adsorption time step, along with the 2 µmol/mol limit required for fuel-cell-grade hydrogen (dashed black line); b) CO content in the outlet hydrogen product stream as a function of adsorption time step, along with the 0.2 µmol/mol limit required for fuel-cell-grade hydrogen (dashed black line).

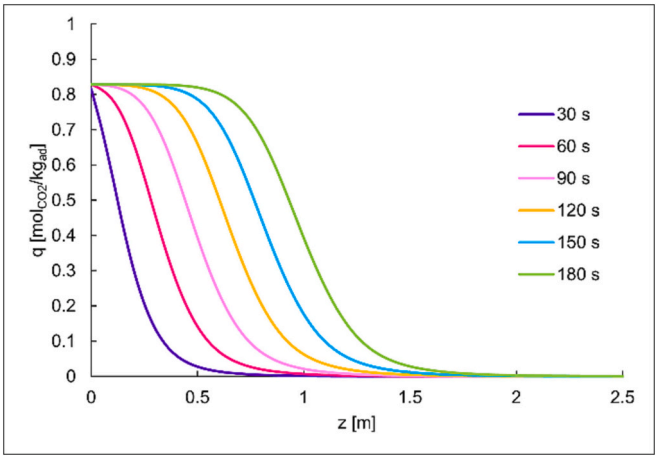

Fig. 5. CO_2 adsorbed on the sorbent as a function of the column length at various adsorption time step. Total reactor length: 2.5 m.

spent along the column length, the concentration profile of impurities is shifted forward. This shift reduces the available length for CO_2 adsorption and, therefore, hinders the conversion of CO by the sorption-enhancing effect.

For example, Fig. 4a-b shows that the base case adsorption time (180 s) results in too high levels of CO_2 and CO impurities. Lowering the adsorption time to 120 s allowed the achievement of the CO specification, but the 2 µmol/mol limit for CO_2 is only met at 60 s. Consequently, the adsorption time was set to 60 s (corresponding to a 30 s time step duration), resulting in compositions of 0.705 µmol/mol for CO_2 and

Table 5
CO_2 and CO content in the hydrogen product stream resulting from sensitivity analyses simulating variations of feed flowrate and feed CO_2 content.

Residual content in H_2-Product Stream	Base Case Feed Conditions	5% Increase in Feed Flowrate	5% Decrease in Feed Flowrate	5% Increase in the Molar Fraction of CO_2 at the Feed
CO_2 [µmol/mol]	0.705	1.21	0.375	0.442
CO_2 variation compared to base case [%]	/	+72%	−47%	−37%
CO [µmol/mol]	0.0158	0.0280	0.00839	0.00816
CO variation compared to base case [%]	/	+79%	−47%	−48%

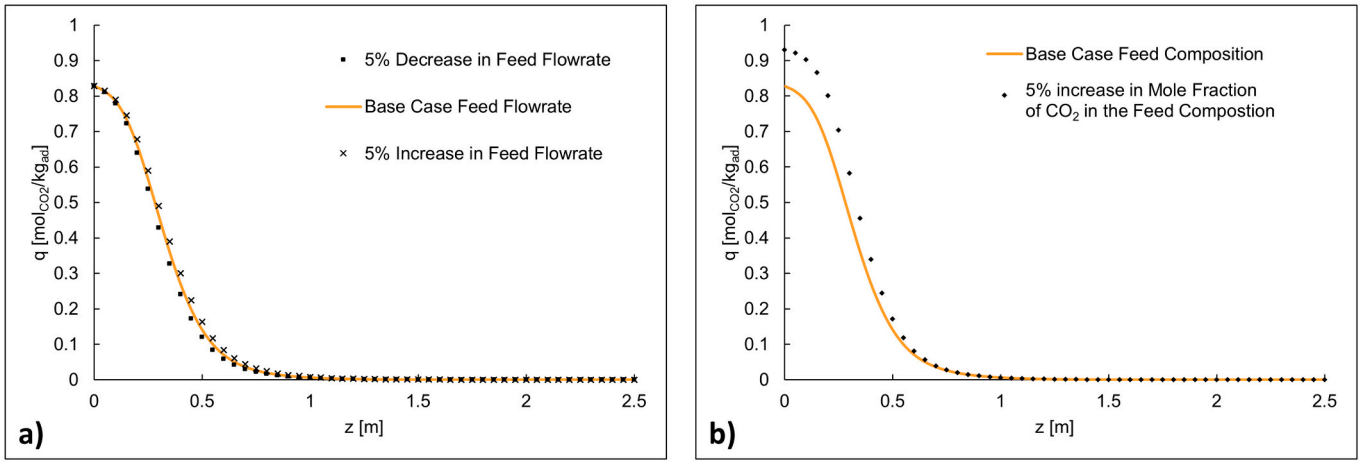

Fig. 6. a) CO_2 adsorbed on the sorbent as a function of the column length at the end of the adsorption step at various feed flowrate; b) CO_2 adsorbed on the sorbent as a function of the column length at the end of the adsorption step with increased CO_2 content in the feed. Adsorption time of 60 s. Total reactor length: 2.5 m.

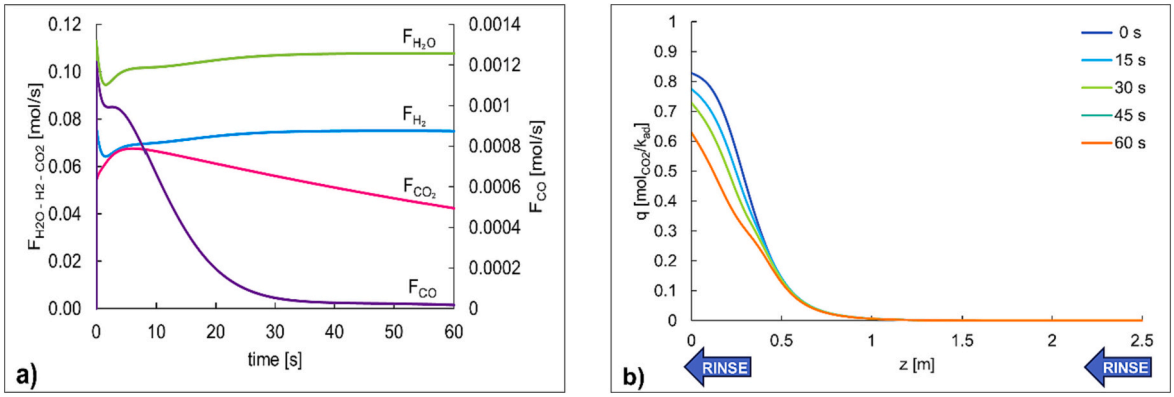

Fig. 7. a) Outlet molar flowrate of components in the rinse step as a function of time in the counter-current configuration; b) CO_2 adsorbed along the column in the rinse step over time in the counter-current configuration. Rinse time of 60 s.

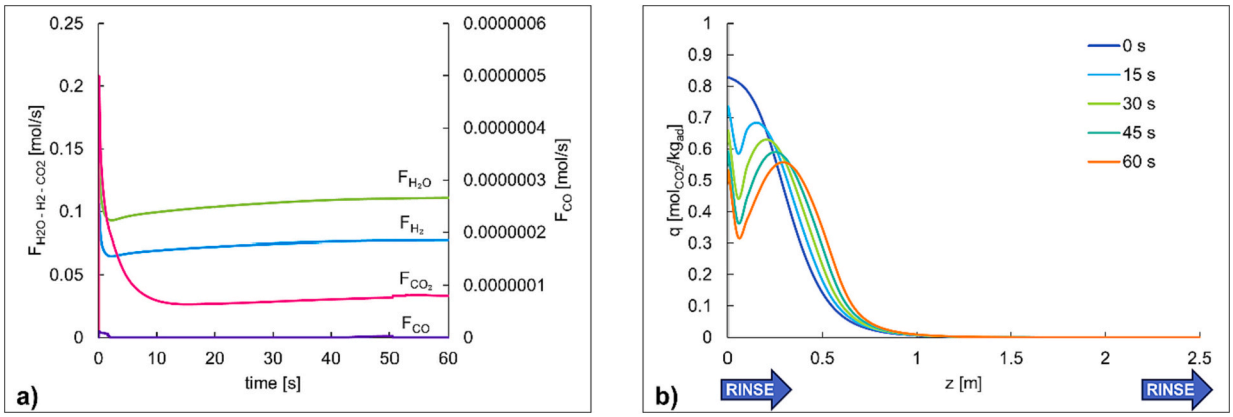

Fig. 8. a) Outlet molar flowrate of components in the rinse step as functions of time in the co-current configuration; b) CO_2 adsorbed as a function of reactor length at several rinse times in the co-current configuration. Rinse time of 60 s. Total reactor length: 2.5 m.

0.0158 μmol/mol for CO in the hydrogen product stream.

Further reducing the time step duration would be sensible in practice, considering the expected increase in these values during continuous operation in case of partial sorbent regeneration. However, decreasing the time step also reduces the available time for rinse and purge steps, imposing higher steam consumption. This significantly impacts the process's economics, efficiency, and environmental burden.

In addition to evaluations of adsorption duration, changes to the feed properties were evaluated to assess the system's sensitivity to disturbances, which are common in waste fuelled plants. A ± 5% variation was imposed to the syngas flowrate to the column and simulated (Fig. 6a): no significant changes in the column's adsorption profile resulted, with a slight shift forward in the adsorption front for increased flow given the higher overall quantity of CO_2 fed to the reactor (while the reverse occurred for decreased flow). The most significant change occurred in CO_2 content in the hydrogen product, with values of +72%

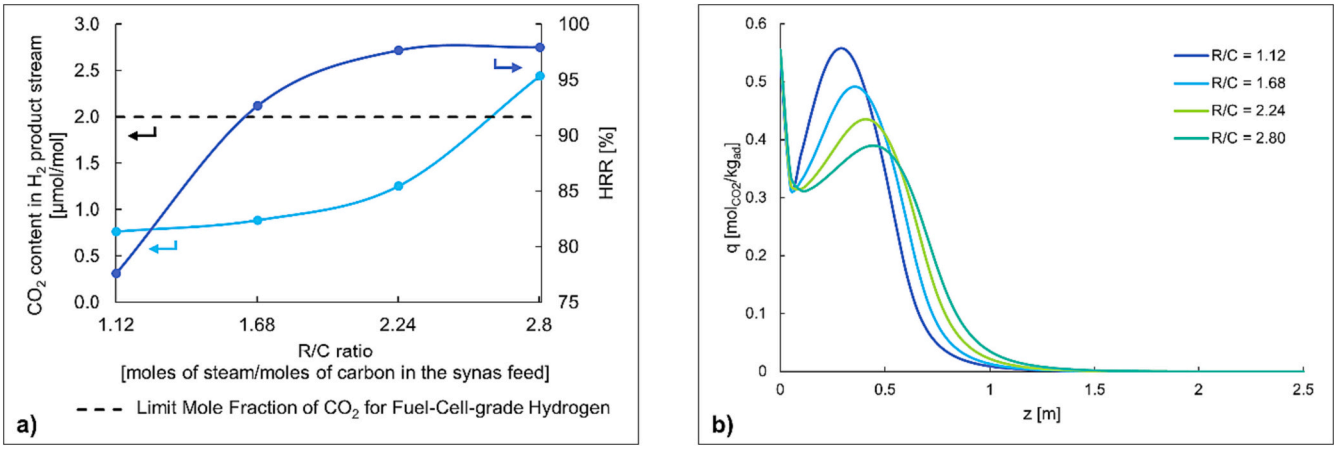

Fig. 9. a) HRR and mole fraction of CO_2 in the hydrogen product stream as functions of various rinse steam flowrate in a co-current configuration; b) CO_2 adsorbed as a functions of reactor length at several steam flowrate in the co-current configuration. Rinse time of 60 s. Total reactor length: 2.5 m.

for higher feed flowrate, and − 47% at lower feed flowrate, all having the base case as a reference (Table 5). This is expected, as with increased feed flowrate, the residence time available for CO_2 to both adsorb on the sorbent and react with steam decreases. Since the partial pressures of all components were not varied, the WGS reaction rate and the adsorption rate of CO_2 remain relatively the same as in the base case, explaining the minor change observed in the adsorption profile and the increased CO_2 content at the outlet. The opposite effects occur with decreased flowrate. These conclusions are further supported by the variation in the CO content at the product stream with varying flowrate, which is seen to change by a similar degree to that observed with the CO_2 mole fraction.

A sensitivity analysis was performed also concerning the CO_2 content in the feed, assuming a + 5% increase. Interestingly, the results show a significant decrease in CO_2 (−37%) and CO (−48%) content at the outlet compared to the base case (Table 5). However, Fig. 6b reveals a notable increase in adsorbed CO_2 at the inlet bed portion, possibly due to the higher CO_2 partial pressure. This leads to enhanced equilibrium adsorption isotherm, resulting in increased adsorption rate. Furthermore, the higher amount of adsorbed CO_2 results to an increased forward WGS reaction rate, reducing the residual CO in the H_2 product stream.

3.2. Rinse step

The adsorption step achieves only a 46.8% of HRR, with the selected counter-current configuration in the base case, significantly compromising the system's efficiency and potentially impacting the CO_2 product's CP. Ideally, the stream generated in the rinse step should be merged with the hydrogen product. However, based on Fig. 7a, it can be concluded that is not possible, due to the large amount of CO_2 that would leave the column. At the end of the adsorption step, the CO_2 content in the gas phase mainly concentrates at the bottom of the column, due to the higher CO_2 concentration in the syngas feed and the fact that the sorbent at the bottom might be already saturated. Therefore operating with a counter-current configuration in the rinse step, the steam flow will not only directly carry the CO_2 content in the gas phase to the outlet, but also push the front of adsorbed CO_2 forward, causing the desorbed CO_2 to end up in the product stream, as shown Fig. 7b.

Interestingly, by changing to co-current rinse configuration, the CO_2 content exiting the column become negligible (Fig. 8a). In co-current mode, steam is introduced at the concentrated CO_2 region (reactor bottom), pushing upward both CO_2 already in gaseous phase and newly desorbed CO_2, towards sorbent layers with lower CO_2 loading at the end of adsorption phase; this resulted in a transient adsorption front, peaking along the column (Fig. 8b). This effectively prevents contamination of the hydrogen product stream, making unspent bed layers working as an additional purification guard.

The impact of steam flowrate in a co-current rinse configuration on system performance was assessed by a sensitivity analysis: the steam flowrate was increased in the rinse step by 50% increments (R/C = 1.68, 2.24, 2.8) compared to the base case (R/C = 1.12) and analysing its effects on HRR and CO_2 content in the hydrogen product (combining adsorption and rinse steps). Fig. 9 shows the results of this sensitivity analysis. At the base case (1.12 R/C ratio), the co-current rinse improves the HRR up to 77.6% (vs. 46.8 of the counter-current rinse), with a CO_2 content in H_2 product of 0.8 μmol/mol (Fig. 9). Higher steam flowrates lead to further HRR improvements, eventually plateauing at R/C ratios exceeding 2.24. However, the outlet CO_2 mole fraction increases more than linearly with the R/C ratio, resulting in a significant shift forward with respect to the column length of the adsorption front, calculated at the end of the rinse step (Fig. 9b). Consequently, at an R/C ratio of 2.80, the CO_2 content in the hydrogen product exceeds the specified limit, making it impractical to incorporate the rinse effluent stream into the hydrogen product.

Therefore, a co-current configuration with a R/C ratio of 2.24 resulted as the optimal arrangement for the rinse step, which allows for a HRR of 97.7%, while maintaining the CO_2 mole fraction in the hydrogen product at 1.2 μmol/mol, below its limit for PEM fuel cell applications. Choosing a higher steam flow would not be advisable since it would result in CO_2 content approaching or exceeding that limit, without any significant gain in HRR that would justify the increased steam consumption costs. A lower value, for example R/C of 1.68 was also acceptable, given the relatively high HRR of 92.7% and the lower CO_2 contamination in the hydrogen product (0.9 μmol/mol), along with the reduced steam consumption costs. However, it is common practice in SEWGS and related processes to aim for a hydrogen recovery rate higher than 95% to enhance efficiency, economic returns, and achieve high CO_2 purity for carbon capture and storage applications [25,57,58].

3.3. Purge step

The effect of steam flowrate on CO_2 removal and sorbent regeneration was studied during the purge step, by a sensitivity analysis that involved increments of steam flowrate by 100% relative to the base case (P/C = 1). The impact on sorbent regeneration resulted low, becoming negligible for P/C ratio of 3 or higher (Fig. 10a). The main effect of steam flow is in rinsing out the gas phase CO_2, as shown in Fig. 10b. However, the efficiency of gaseous CO_2 removal gradually decreases with higher flowrates because the lower partial pressure of CO_2 along the column leads to increased desorption, resulting in more CO_2 in the gas phase.

The purge step's inefficiency is even more evident when evaluating

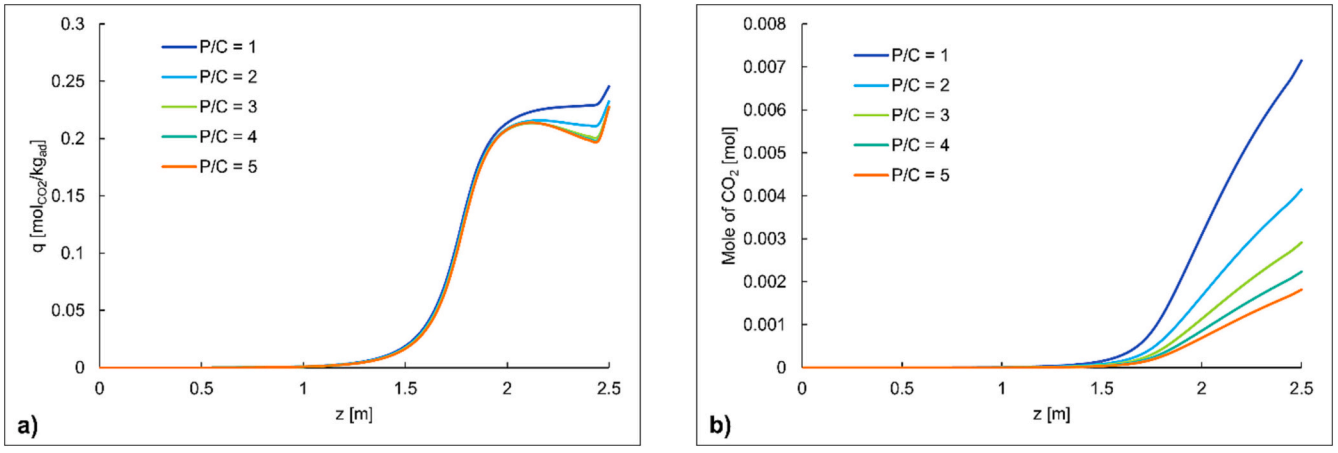

Fig. 10. a) CO_2 adsorbed as a function of reactor length at several steam flowrates; b) Gas phase CO_2 content as a function of reactor length at several steam flowrates. Purge time of 60 s. Total reactor length: 2.5 m.

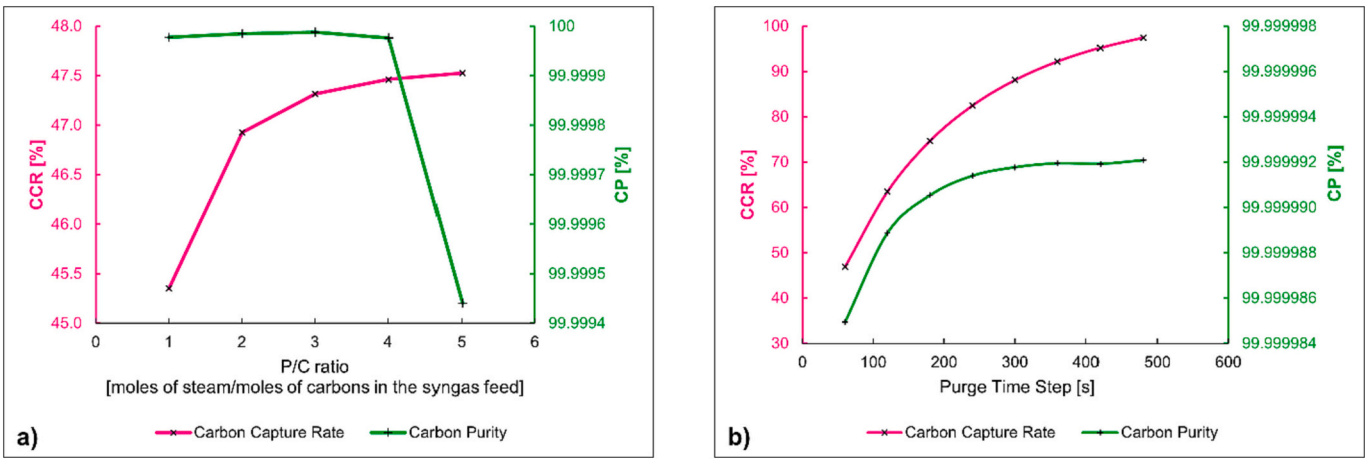

Fig. 11. a) CCR and CP in the CO_2 product stream as a functions of different steam flowrates. Purge time of 60 s; b) CCR and CP in the CO_2 product stream as a function of different purge time step, P/C ratio of 2.

Table 6
Design parameters adopted for the fully cycle simulation.

	A	R	PE_d	BD	R	PE_p	RP	R/C ratio	2.24
Step duration [s] (t_{step} - 30 s)	60	60	30	30	420	30	30	**P/C ratio**	2

Table 7
Results for the full cycle operation of the SEWGS pilot process.

	Dry Hydrogen Product			Dry Carbon Dioxide Product	
	y_{CO2} [μmol/mol]	HRR [%]	HP [%]	CCR [%]	CP [%]
Cycle 1	1.25	97.6	99.9	95.2	99.9
Cycle 2	5.90	88.5	99.5	97.2	99.9
Cycle 3	7.00	88.5	99.5	97.4	99.9
Cycle 4	7.24	88.5	99.5	97.5	99.9
Cycle 5	7.40	88.5	99.5	97.4	99.9
Cycle 6	7.40	88.5	99.5	97.4	99.9

the CCRs and CPs, as shown in Fig. 11a. There is a minor increase in CCR with higher steam flow, but it becomes even more negligible above a P/C ratio of 2. The overall CCR obtained remains low in all examined cases (<50%), indicating that approximately half of the fed CO_2 remains adsorbed even after the purge step. This suggests that the sorbent could become saturated after a few cycles, making the purge step impractical, despite always achieving high CPs suitable for CCS applications (impurities in recovered CO_2 always <0.001%). The effect of purge step duration on CCR and CP was evaluated at a P/C ratio of 2 over different time intervals (Fig. 11b): increasing the purge time improves sorbent regeneration. However, to ensure optimal sorbent cyclic working capacity and minimize impurities content in the hydrogen product, a CCR of 95% or higher is required, which is only achieved at a purge step duration of 420 s. This presents challenges as it hinders continuous hydrogen production by a five-columns-stack and significantly increases steam consumption, necessitating an overall P/C ratio of 14. This would have a substantial impact on the process economics and environment on a full-scale pilot plant. However, for the only sake of pilot plant operation, this is shown to be the only viable option to meet the required product specifications.

3.4. Fully cycle operation

Simulations for the full cyclic operation of the process were performed by the single bed approach, to evaluate long-term performance. The formulations for HRR and CCR had to be modified, to account for the H_2 and CO_2 gases present in the column and the CO_2 adsorbed on the sorbent after each cycle, as given by Eq. (15) and Eq. (16), respectively.

$$HRR_{tot} = \frac{\sum_j \int_0^{t_j} y_{H_2,out,j}\, F_{out,j}\, dt}{\left(y_{H_2,Feed} + y_{CO,Feed}\right) F_{Feed}\, t_A + \int_0^{L} \frac{dN_{H_2,0}}{dz} dz} \times 100 \tag{15}$$

$$CCR_{tot} = \frac{\sum_k \int_0^{t_k} y_{CO_2,out,k}\, F_{out,k}\, dt}{\left(y_{CO_2,Feed} + y_{CO,Feed}\right) F_{Feed}\, t_A + \int_0^{L} \frac{dN_{CO_2,0}}{dz} dz + \int_0^{L} q_{CO_2} A_c \rho_{b,ads} \left(1 - \varepsilon_b\right) dz} \times 100 \tag{16}$$

Based on the previous analyses, the optimal configuration for the SEWGS process includes co-current rinse operation, with the stream generated during this step directly incorporated into hydrogen product stream. Table 6 summarise the design parameters adopted for the simulations. Six full cycles were simulated in series, the results of which are given in Table 7. It should be noted that only the first cycle works with fresh sorbent at full capacity.

Table 7 shows that after an initial drop in performance on HRR from Cycle 1, a constant value of 88.5% is obtained from Cycle 2 to Cycle 6.

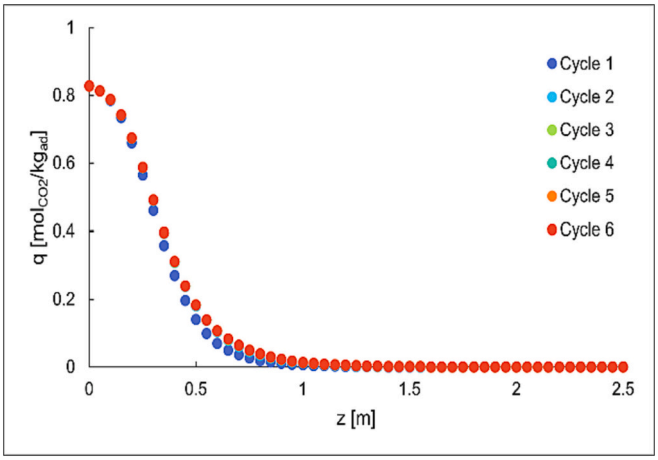

Fig. 12. CO_2 adsorbed as a function of reactor length at the end of the adsorption step for the various full cycle simulations.

The decreasing in HRR value is caused by the residual CO_2 adsorbed on the sorbent, which reduces the CO_2 adsorption rate, hence lowering the sorption-enhancing effect on WGS. The CO_2 content in the hydrogen product undergoes a gradual increase with each cycle run with a coupled decrease of HP, also resulting from the lower CO_2 adsorption rate along the column. This trend with cycles makes the hydrogen product go outside the fuel-cell-grade specifications required, from Cycle 2 and beyond, meaning that the process will have to be modified to meet this target, either by incorporating an additional hydrogen purification step or altering the operating conditions set. Regarding the CO_2 product, a slight improvement was obtained for CCR, which is associated with the greater amount of CO_2 adsorbed on the sorbent following Cycle 1, as shown in Fig. 12, that results in an increased desorption rate at the blow down and purge steps. Moreover, from the convergence in the CCR achieved and in the CO_2 obtained in the hydrogen product after multiple cycle runs, we can conclude that steady state is reached and full sorbent saturation is avoided in the process, as can also be deduced from the relatively constant adsorption profile displayed in Fig. 12. As for the purity of the CO_2 product, the fluctuations are negligible over multiple cycles. However, extremely high CPs are still generated from the process, which exceed the CCS-grade specifications required.

Table 8: summarizes a comparative investigation between the results obtained in this work and those from other SEWGS and related processes from literature: the system simulated in this work achieved a superior separation of H_2 and CO_2, obtaining a considerably high purity for both products (Table 8, HP = 99.5%, CP = 99.9%), even surpassing the HP reached by Zhu et al. (2018) [57] through an elevated-temperature pressure swing adsorption (ET-PSA) process, in contrast with the low HRR (89.0%. Table 8). However, the high purity always comes at the cost of recovery: when fixing the bed number, this phenomenon is commonly observed with operating parameters including adsorption pressure, adsorption time, feed flowrate, purge rate, purge-to-feed ratio, cycle time and adsorbent loading ratio in layered bed [46].

Despite the lower HRR, the CP obtained was still extremely high, particularly compared with other SEWGS processes that recovered a considerably higher percentage of hydrogen (Table 8). This is due to the lower hydrogen-to-carbon ratio present in waste syngas feed compared to that obtained in syngas streams generated from coal and natural gas feedstocks [25,41,59]. These observations may suggest that biomass-rich feedstocks could allow for higher HPs (at the cost of having a lower HRR), without compromising the purity of the CO_2 product. Consequently, SEWGS offers greater opportunity to BECCS and low-carbon hydrogen production, compared to other solutions.

Another important point to consider is the large steam consumption (Table 8, R/C and P/C ratios) in the current pilot, compared to literature. This is related to several aspects that must be considered:

- the lower-than-average number of pressure equalization steps in the investigated pilot process, which increases the steam demand in the rinse step [24,60]. It has been demonstrated that increasing the number of equalization steps enabled the rinse steam to be reduced without significantly changing the purge steam, as it reduced the H_2 remaining inside the bed before the blow down step [46,61];

Table 8
Comparison of the results obtained in this work with those achieved by SEWGS and related process from literature, as well as contrasting between the different configurations of each process.

	This work	Reijers et al. (2011) [59]	Boon et al. (2015) [24]	Najmi et al. (2016) [41]	Wright et al. (2009) [25]	Zhu et al. (2018) [57]
Process	SEWGS 5-column 7-steps (co-current rinse)	SEWGS 6-column 8-steps (counter-current rinse)	SEWGS 9-column 11-steps (co-current rinse)	SEWGS 8-column 11-steps (counter-current rinse)	SEWGS 8-column 11-steps (counter-current rinse)	ET-PSA 8-column 13-steps (co-current rinse)
HP [%]	99.5	93.2[a]	76.8[a]	81.1	46.5	97.7
HRR [%]	88.5	99[a]	95[a]	–	99	98
CP [%]	99.9	98.0	99.0	99.3	99.9	–
CCR [%]	97.4	90	95	95	91	–
R/C ratio	2.24	0.55	0.03	0.4	0.89	0.56
P/C ratio	14	1.3	0.08	1.5	1.33	1.0
t_{step} Duration [s]	30	–	38	44	–	60
Adsorption t_{step} [s]	60	–	156	174	–	90
Purge t_{step} [s]	420	–	156	87	–	240
Set of Pressure Equalization Step	1	1	3	3	3	4
Operating Pressure Range [bar]	12–1.1	23.6–2.0	24.0–1.1	27.0–1.0	28.0–1.1	30.4–1.2
Operating Temperature [°C]	350	400	400	400	400	400
Feed Composition	29.5% H_2 2.3% CO 20.0% CO_2 47.9% H_2O 0.30% N_2	32.6% H_2O 34.6% H_2 4.7% CO 23.8% CO_2	0.8% Ar 27.6% H_2O 3.6% H_2 7.1% CO 54.4% CO_2 6.5% N_2	3.46% CO_2 22.06% H_2 49.33% CO 18.17% H_2O 6.98% N_2	2.6% CO 15.2% H_2O 11.7% CO_2 32.2% H_2 38.2% Inert gas	40% H_2 1% CO 30% CO_2

[a] Hydrogen product results were obtained from Zhu et al. (2018) [57].

- the adsorption step duration is well below that adopted in any other process (Adsorption t_{step}: 60 s, Table 8). Recall that this step duration was reduced to ensure optimal HP and minimal impurities content in the hydrogen product, in contrast, the P/C ratio and purge step duration had to be increased considerably to enhance sorbent regeneration for high-purity hydrogen to be obtained (Table 8);
- the operating pressure range and operating temperature used in the current process are lower than in the literature (Table 8, operating pressure range [bar]: 12–1.1, operating temperature [°C]: 350), which limit the cyclic working capacity of the sorbent and may contribute to higher steam requirement.

From this study, it seems that a 5-column SEWGS may not be a viable method of producing fuel-cell-grade hydrogen without the incorporation of an additional hydrogen purification step or a multi-train configuration, particularly considering the extreme steam demands required to do so. However, the same system is effective in producing hydrogen for heating applications, which requires lower hydrogen purity of 98% and could accommodate higher quantities of other impurities, such as methane, sulphur, etc. [56].

4. Conclusions

The increasing concern with climate change is leading a global transition towards renewable and low-carbon energies, in which BECCS is expected to play a crucial role in offsetting GHG emissions. Recently, with the emerging investment in hydrogen production and CCS technologies, SEWGS has gained increasing attention as an intensification process for simultaneous carbon capture and hydrogen generation, aiming to reduce capital costs and energy demands. This study has analysed and optimised a 5-column SEWGS pilot unit, set to operate for the first time in a waste gasification facility. From the sensitivity analysis performed, syngas flowrate variations were seen to have an instantaneous, but temporary, impact on hydrogen product specifications, while changes to syngas composition were deduced to have a longer-lasting effect on performance. Based on full cycle operation results, the current SEWGS unit design was concluded to be inadequate for fuel-cell-grade H_2 production, despite obtaining a high HP of 99.5%, mainly due to its excessive steam consumption. Nevertheless, compared with literature results, the process achieved an exceptionally high CP of 99.9%, despite the relatively low 88.6% HRR obtained. This indicated that the incorporation of SEWGS in BECCS may allow for higher purity hydrogen products to be obtained, whilst meeting CCS product specifications, in contrast with using fossil-based feedstocks, although mostly for heating applications. Overall, this study has contributed towards a deeper understanding of SEWGS as a pre-combustion carbon capture technology for BECCS and a high-purity hydrogen production method, both of which are increasingly important topics, with still limited available research.

Nomenclature

Abbreviations

A	adsorption step in SEWGS cycle
BECCS	bioenergy with carbon capture and storage
BD	blow down step in SEWGS cycle
bioSNG	bio synthetic natural gas
CP	carbon purity
CCR	carbon capture ratio
CCS	carbon capture and storage
DMEA	dimethylethanolamine
ET-PSA	elevated temperature pressure swing adsorption
GHG	greenhouse gas emission
HP	hydrogen purity
HRR	hydrogen recovery rate
HTS	high temperature shift
IEA	international energy agency
IGCC	integrated gasification combined cycle
K-HTC	potassium-promoted hydrotalcite
LDF	linear driving force
LTS	low temperature shift
MEA	monoethanolamine
MTH	methanation step
ODEs	ordinary differential equations
P	purge step in SEWGS cycle
P/C	purge to carbon ratio
PDEs	partial differential equations
PE_d	pressure equalization depressurization step in SEWGS cycle
PE_p	pressure equalization pressurization step in SEWGS cycle
PSA	pressure swing adsorption
R	rinse step in SEWGS cycle
R/C	rinse to carbon ratio
RP	repressurization step in SEWGS cycle
RDF	refuse derived fuel
SEWGS	sorption-enhanced water-gas shift
WGS	water-gas shift

Symbols

A	nanopore-sorbate interaction parameter, –
A_c	column cross-sectional area, m^2
c	molar concentration, mol m^{-3}
d_p	particle diameter, m
d_r	reactor internal diameter, m
D_{ax}	axial mass dispersion coefficient, m^2 s
D_m	molecular diffusivity of the gas mixture, m^2 s
$D_{m,i}$	molecular diffusivity of the gas component i, m^2 s
D_p	intraparticle diffusion coefficient, m^2 s
E	nanopore-sorbate interaction energy, J mol^{-1}
F	molar flow rate, mol s^{-1}
K	surface-sorbate interaction parameter, Pa^{-1}
K_{eq}	equilibrium constant for the WGS reaction
K_D	Ergun equation coefficient, N s m^{-4}
K_V	Ergun equation coefficient, N s^2 m^5
k	rate constant for the WGS reaction, mol g_{cat}^{-1} h^{-1} Pa^{-2}
k_{LDF}	linear driving force intraparticle mass transfer coefficient, s^{-1}
L	reactor length, m
M_{av}	average molar mas of gas mixtures, kg mol^{-1}
m	pore-size distribution parameter, –
N_i	mole number of chemical species i, mol
p	pressure, Pa
p_i	partial pressure of species i, Pa
p_c	critical pressure, Pa
p_H	high pressure in cycle simulation, Pa
p_I	intermediate pressure in cycle simulation, Pa
p_L	low pressure in cycle simulation, Pa
p_0	saturation pressure, Pa
q	solid phase adsorption capacity, mol_{CO2} kg_{ad}^{-1}
q^{eq}	equilibrium solid phase concentration, mol kg^{-1}
q^s	maximum concentration adsorbed, mol kg^{-1}
R	universal gas constant, J mol^{-1} K^{-1}
r_{wgs}	water-gas shift reaction rate, mol g_{cat}^{-1} h^{-1}
T	temperature, K
t	time, s
T_c	critical temperature, K
u	superficial gas velocity, m s^{-1}
v_m	molar volume, cm^3 mol^{-1}
V_0	limiting nanopore volume per mass of sorbent, cm^3 kg^{-1}
y_i	gas phase mole fraction of species i, –
z	column axial coordinate, m

Greek

ε_b	bed void fraction, –
ε_p	adsorbent porosity, –
ε_t	total bed porosity, –
$\rho_{b,ads}$	bulk density of adsorbent, kg m^{-3}
$\rho_{b,cat}$	bulk density of catalyst, kg m^{-3}
ρ_p	particle density, kg m^{-3}
ρ_g	gas-phase density, kg m^{-3}
μ	viscosity of the fluid, Pa s

Subscribes

0	initial
i	generic chemical species
j	step contributing to hydrogen product stream
k	step contributing to carbon dioxide product stream
out	outlet
tot	total

CRediT authorship contribution statement

Barbara Malsegna: Data curation, Investigation, Visualization, Writing – original draft. **Alex Sebastiani:** Data curation, Investigation, Validation. **João Guilherme da Gama Paz-Dias:** Formal analysis, Methodology, Validation. **Francesco Di Luca:** Data curation, Formal analysis, Supervision, Project administration, Resources. **Andrea Di Giuliano:** Formal analysis, Data curation, Methodology, Supervision, Writing – review & editing. **Katia Gallucci:** Data curation, Formal analysis, Supervision, Funding acquisition, Supervision, Writing – review & editing. **Massimiliano Materazzi:** Conceptualization, Formal analysis, Investigation, Supervision, Writing – review & editing.

Declaration of competing interest

The authors declare the following financial interests/personal relationships which may be considered as potential competing interests:

Barbara Malsegna reports financial support was provided by MUR (Italian Ministry of University and Research).

Data availability

Data will be made available on request.

Acknowledgements

This work was supported by MUR (Italian Ministry of University and Research) [PON 2014-2020 – CUP E19J21012860001 – DOT13LHQ8Y-2].

The authors wish to acknowledge the contribution of Andy Cornell and Richard Taylor from Advanced Biofuel Solutions (ABSL) for providing access to Swindon plant data and for the insightful discussion throughout the project.

Appendix A. Supplementary data

Supplementary data to this article can be found online at https://doi.org/10.1016/j.fuproc.2024.108032.

References

[1] IEA, World Energy Outlook 2022. www.iea.org/t&c/, 2022.
[2] M. Materazzi, S. Chari, A. Sebastiani, S. Bajwa, Waste-to-hydrogen: challenges and opportunities in the UK scenario, Detritus. 23 (2023) 65–75, https://doi.org/10.31025/2611-4135/2023.18274.
[3] S. Masoudi Soltani, A. Lahiri, H. Bahzad, P. Clough, M. Gorbounov, Y. Yan, Sorption-enhanced steam methane reforming for combined CO2 Capture and hydrogen production: a state-of-the-art review, carbon capture, For. Sci. Technol. 1 (2021) 100003, https://doi.org/10.1016/j.ccst.2021.100003.
[4] G. Amaya-Santos, S. Chari, A. Sebastiani, F. Grimaldi, P. Lettieri, M. Materazzi, Biohydrogen: a life cycle assessment and comparison with alternative low-carbon production routes in UK, J. Clean. Prod. 319 (2021) 128886, https://doi.org/10.1016/J.JCLEPRO.2021.128886.
[5] A. Ajanovic, M. Sayer, R. Haas, The economics and the environmental benignity of different colors of hydrogen, Int. J. Hydrog. Energy 47 (2022) 24136–24154, https://doi.org/10.1016/J.IJHYDENE.2022.02.094.
[6] E.S. Rubin, H. Mantripragada, A. Marks, P. Versteeg, J. Kitchin, The outlook for improved carbon capture technology, Prog. Energy Combust. Sci. 38 (2012) 630–671, https://doi.org/10.1016/J.PECS.2012.03.003.
[7] L.C. Wirner, F. Kosaka, T. Sasayama, Y. Liu, A. Urakawa, K. Kuramoto, Combined capture and reduction of CO2 to methanol using a dual-bed packed reactor, Chem. Eng. J. 470 (2023), https://doi.org/10.1016/j.cej.2023.144227.
[8] P. Balcombe, J. Speirs, E. Johnson, J. Martin, N. Brandon, A. Hawkes, The carbon credentials of hydrogen gas networks and supply chains, Renew. Sust. Energ. Rev. 91 (2018) 1077–1088, https://doi.org/10.1016/J.RSER.2018.04.089.
[9] M. Shahbaz, A. AlNouss, I. Ghiat, G. Mckay, H. Mackey, S. Elkhalifa, T. Al-Ansari, A comprehensive review of biomass based thermochemical conversion technologies integrated with CO2 capture and utilisation within BECCS networks, Resour. Conserv. Recycl. 173 (2021) 105734, https://doi.org/10.1016/J.RESCONREC.2021.105734.
[10] K. Gallucci, A. Di Giuliano, S. Rapagnà, Steam O2-enriched air gasification of lignite and solid recovered fuel in fluidized bed, Fuel. 303 (2021), https://doi.org/10.1016/j.fuel.2021.121271.
[11] BECCS: The Carbon Capture Technology the UK is Relying on to Reach Net Zero. https://theconversation.com/beccs-the-carbon-capture-technology-the-uk-is-relying-on-to-reach-net-zero-182176, 2022 (accessed October 25, 2022).
[12] C. Gough, S. Garcia-Freites, C. Jones, S. Mander, B. Moore, C. Pereira, M. Röder, N. Vaughan, A. Welfle, Global Sustainability challenges to the use of BECCS as a keystone technology in pursuit of 1.5°C, Glob. Sustain. 1 (2018) 1–9, https://doi.org/10.1017/sus.2018.3.
[13] M. Materazzi, P.U. Foscolo, The role of waste and renewable gas to decarbonize the energy sector, in: Substitute Natural Gas from Waste: Technical Assessment and Industrial Applications of Biochemical and Thermochemical Processes, Elsevier, 2019, pp. 1–19, https://doi.org/10.1016/B978-0-12-815554-7.00001-5.
[14] C. Acar, I. Dincer, Comparative assessment of hydrogen production methods from renewable and non-renewable sources, Int. J. Hydrog. Energy 39 (2014) 1–12, https://doi.org/10.1016/j.ijhydene.2013.10.060.
[15] H. Tian, J. Li, M. Yan, Y.W. Tong, C.H. Wang, X. Wang, Organic waste to biohydrogen: a critical review from technological development and environmental impact analysis perspective, Appl. Energy 256 (2019), https://doi.org/10.1016/j.apenergy.2019.113961.
[16] Technology Roadmap - Hydrogen and Fuel Cells – Analysis - IEA, IEA, 2015. https://www.iea.org/reports/technology-roadmap-hydrogen-and-fuel-cells (accessed October 10, 2023).
[17] M. Materazzi, R. Taylor, M. Cairns-Terry, Production of biohydrogen from gasification of waste fuels: pilot plant results and deployment prospects, Waste Manag. 94 (2019) 95–106, https://doi.org/10.1016/J.WASMAN.2019.05.038.
[18] S. Budinis, S. Krevor, N. Mac Dowell, N. Brandon, A. Hawkes, An assessment of CCS costs, barriers and potential, Energ. Strat. Rev. 22 (2018) 61–81, https://doi.org/10.1016/J.ESR.2018.08.003.
[19] V.S. Sikarwar, C. Pfeifer, F. Ronsse, M. Pohořelý, E. Meers, A.K. Kaviti, M. Jeremiáš, Progress in in-situ CO2-sorption for enhanced hydrogen production, Prog. Energy Combust. Sci. 91 (2022), https://doi.org/10.1016/j.pecs.2022.101008.
[20] N. Zecca, P.D. Cobden, L. Lücking, G. Manzolini, SEWGS Integration in a Direct Reduction Process for CO 2 Mitigation. https://ssrn.com/abstract=4493859, 2023.
[21] A.E. Rodrigues, L.M. Madeira, Y.-J. Wu, R. Faria, Sorption Enhanced Reaction Processes, 01, 2017, https://doi.org/10.1142/Q0103.
[22] S. Karagöz, Huanhao Chen, M. Cao, T. Tsotsis Theodore, I. Manousiouthakis Vasilios, Multiscale Model Based Design of an Energy-Intensified Novel Adsorptive Reactor Process for the Water Gas Shift Reaction, 2019, https://doi.org/10.1002/aic.16608.
[23] S. Decker, J. Tian, T.J. Stadler, J.-H. Knoop, P. Pfeifer, Numerical Simulation Approach for a Dynamically Operated Sorption-Enhanced Water-Gas Shift Reactor, 2022, https://doi.org/10.3390/pr10061160.
[24] J. Boon, P.D. Cobden, H.A.J. van Dijk, M. van Sint Annaland, High-temperature pressure swing adsorption cycle design for sorption-enhanced water-gas shift, Chem. Eng. Sci. 122 (2015) 219–231, https://doi.org/10.1016/j.ces.2014.09.034.
[25] A. Wright, V. White, J. Hufton, E. van Selow, P. Hinderink, Reduction in the cost of pre-combustion CO2 capture through advancements in sorption-enhanced water-gas-shift, Energy Procedia 1 (2009) 707–714, https://doi.org/10.1016/j.egypro.2009.01.093.
[26] J. Boon, P.D. Cobden, H.A.J. van Dijk, C. Hoogland, E.R. van Selow, M. van Sint Annaland, Isotherm model for high-temperature, high-pressure adsorption of CO2 and H2O on K-promoted hydrotalcite, Chem. Eng. J. 248 (2014) 406–414, https://doi.org/10.1016/j.cej.2014.03.056.
[27] H.A.J. van Dijk, S. Walspurger, P.D. Cobden, D. Jansen, R.W. van den Brink, F. G. de Vos, Performance of water-gas shift catalysts under sorption-enhanced water-gas shift conditions, in: Energy Procedia, Elsevier, 2009, pp. 639–646, https://doi.org/10.1016/j.egypro.2009.01.084.
[28] H.A.J. van Dijk, S. Walspurger, P.D. Cobden, R.W. van den Brink, F.G. de Vos, Testing of hydrotalcite-based sorbents for CO2 and H2S capture for use in sorption

enhanced water gas shift, Int. J. Greenh. Gas Control. 5 (2011) 505–511, https://doi.org/10.1016/j.ijggc.2010.04.011.
[29] G. Manzolini, A. Giuffrida, P.D. Cobden, H.A.J. van Dijk, F. Ruggeri, F. Consonni, Techno-economic assessment of SEWGS technology when applied to integrated steel-plant for CO2 emission mitigation, Int. J. Greenh. Gas Control. 94 (2020) 102935, https://doi.org/10.1016/j.ijggc.2019.102935.
[30] E.R. Van Selow, P.D. Cobden, A.D. Wright, R.W. Van Den Brink, D. Jansen, Improved sorbent for the sorption-enhanced water-gas shift process, in: Energy Procedia, Elsevier, 2011, pp. 1090–1095, https://doi.org/10.1016/j.egypro.2011.01.159.
[31] E.L.G. Oliveira, C.A. Grande, A.E. Rodrigues, CO2 sorption on hydrotalcite and alkali-modified (K and Cs) hydrotalcites at high temperatures, Sep. Purif. Technol. 62 (2008) 137–147, https://doi.org/10.1016/j.seppur.2008.01.011.
[32] H. Xu, Y. Hu, Z. Cheng, Z. Zhou, Production of high-purity H2 through sorption-enhanced water gas shift over a combination of two intermediate-temperature CO2 sorbents, Int. J. Hydrog. Energy 48 (2023) 25185–25196, https://doi.org/10.1016/j.ijhydene.2023.02.108.
[33] L.K.G. Bhatta, S. Subramanyam, M.D. Chengala, S. Olivera, K. Venkatesh, Progress in hydrotalcite like compounds and metal-based oxides for CO2 capture: a review, J. Clean. Prod. 103 (2015) 171–196, https://doi.org/10.1016/j.jclepro.2014.12.059.
[34] K. Coenen, F. Gallucci, G. Pio, P. Cobden, E. van Dijk, E. Hensen, M. van Sint Annaland, On the influence of steam on the CO2 chemisorption capacity of a hydrotalcite-based adsorbent for SEWGS applications, Chem. Eng. J. 314 (2017) 554–569, https://doi.org/10.1016/j.cej.2016.12.013.
[35] M.H. Halabi, M.H.J.M. De Croon, J. Van Der Schaaf, P.D. Cobden, J.C. Schouten, High capacity potassium-promoted hydrotalcite for CO2 capture in H2 production, Int. J. Hydrog. Energy 37 (2012) 4516–4525, https://doi.org/10.1016/j.ijhydene.2011.12.003.
[36] Y. Hu, H. Cui, Z. Cheng, Z. Zhou, Sorption-enhanced water gas shift reaction by in situ CO2 capture on an alkali metal salt-promoted MgO-CaCO3 sorbent, Chem. Eng. J. 377 (2019), https://doi.org/10.1016/j.cej.2018.08.209.
[37] Y. Hu, Z. Cheng, Z. Zhou, High-purity H2production by sorption-enhanced water gas shift on a K2CO3-promoted Cu/MgO-Al2O3difunctional material, Sustain, Energy Fuel 5 (2021) 3340–3350, https://doi.org/10.1039/d1se00400j.
[38] W.L. Theo, J.S. Lim, H. Hashim, A.A. Mustaffa, W.S. Ho, Review of pre-combustion capture and ionic liquid in carbon capture and storage, Appl. Energy 183 (2016) 1633–1663, https://doi.org/10.1016/j.apenergy.2016.09.103.
[39] M. Materazzi, A. Cornell, P. Cozens, Hydrogen GGR Demonstration Project Project Report, Department for Business, Energy & Industrial Strategyre, 2021, pp. 1–34.
[40] H.T.J. Reijers, J. Boon, G.D. Elzinga, P.D. Cobden, W.G. Haije, R.W. Van Den Brink, Modeling study of the sorption-enhanced reaction process for CO2 capture. I. Model development and validation, Ind. Eng. Chem. Res. 48 (2009) 6966–6974, https://doi.org/10.1021/ie801319q.
[41] B. Najmi, O. Bolland, K.E. Colombo, A systematic approach to the modeling and simulation of a Sorption Enhanced Water Gas Shift (SEWGS) process for CO2 capture, Sep. Purif. Technol. 157 (2016) 80–92, https://doi.org/10.1016/j.seppur.2015.11.013.
[42] A. Di Giuliano, K. Gallucci, F. Giancaterino, C. Courson, P.U. Foscolo, Multicycle sorption enhanced steam methane reforming with different sorbent regeneration conditions: experimental and modelling study, Chem. Eng. J. 377 (2019), https://doi.org/10.1016/j.cej.2018.09.035.
[43] I. Aloisi, A. Di Giuliano, A. Di Carlo, P.U. Foscolo, C. Courson, K. Gallucci, Sorption enhanced catalytic Steam Methane Reforming: experimental data and simulations describing the behaviour of bi-functional particles, Chem. Eng. J. 314 (2017) 570–582, https://doi.org/10.1016/j.cej.2016.12.014.
[44] A. Di Giuliano, K. Gallucci, P.U. Foscolo, Determination of kinetic and diffusion parameters needed to predict the behavior of CaO-Based CO 2 sorbent and sorbent-catalyst materials, Ind. Eng. Chem. Res. 59 (2020) 6840–6854, https://doi.org/10.1021/acs.iecr.9b05383.
[45] B. Malsegna, M. Materazzi, F. Di Luca, A. Di Giuliano, K. Gallucci, Preliminary assessment of sorption capacity on solid CO2-sorbents at conditions for sorption-enhanced processes, Chem. Eng. Trans. 100 (2023) 685–690, https://doi.org/10.3303/CET23100115.
[46] X. Zhu, S. Li, Y. Shi, N. Cai, Recent advances in elevated-temperature pressure swing adsorption for carbon capture and hydrogen production, Prog. Energy Combust. Sci. 75 (2019) 100784, https://doi.org/10.1016/j.pecs.2019.100784.
[47] B. Najmi, O. Bolland, S.F. Westman, Simulation of the cyclic operation of a PSA-based SEWGS process for hydrogen production with CO2 capture, Energy Procedia 37 (2013) 2293–2302, https://doi.org/10.1016/j.egypro.2013.06.110.
[48] G. hua Xiu, J.L. Soares, P. Li, A.E. Rodrigues, Simulation of five-step one-bed sorption-enhanced reaction process, AICHE J. 48 (2002) 2817–2832, https://doi.org/10.1002/aic.690481210.
[49] S. Ergun, Fluid flow through packed columns, Chem. Eng. Prog. 48 (1952) 89–94.
[50] Y. Ding, E. Alpay, Adsorption-enhanced steam–methane reforming, Chem. Eng. Sci. 55 (2000) 3929–3940, https://doi.org/10.1016/S0009-2509(99)00597-7.
[51] Y. Ding, E. Alpay, Equilibria and kinetics of CO2 adsorption on hydrotalcite adsorbent, Chem. Eng. Sci. 55 (2000) 3461–3474, https://doi.org/10.1016/S0009-2509(99)00596-5.
[52] B. Smith, M. Loganathan, M.S. Shantha, A review of the water gas shift reaction kinetics, Int. J. Chem. React. Eng. 8 (2010), https://doi.org/10.2202/1542-6580.2238.
[53] D. Mendes, V. Chibante, A. Mendes, L.M. Madeira, Determination of the low-temperature water− gas shift reaction kinetics using a Cu-based catalyst, Ind. Eng. Chem. Res. 49 (2010) 11269–11279.
[54] W.E. Schiesser, G.W. Griffiths, A Compendium of Partial Differential Equation Models: Method of Lines Analysis with Matlab, Cambridge University Press, 2009. https://books.google.co.uk/books?hl=it&lr=&id=dVcEJsh7524C&oi=fnd&pg=PR7&dq=A+compendium+of+partial&ots=GPVBmyAMgJ&sig=aDjUVzfcj7R27HRd2m-wTYtULsY&redir_esc=y#v=onepage&q=A%20compendium%20of%20partial&f=false (accessed March 29, 2023).
[55] A. Murugan, A.S. Brown, Review of purity analysis methods for performing quality assurance of fuel cell hydrogen, Int. J. Hydrog. Energy 40 (2015) 4219–4233, https://doi.org/10.1016/J.IJHYDENE.2015.01.041.
[56] J.L. Aprea, Quality specification and safety in hydrogen production, commercialization and utilization, Int. J. Hydrog. Energy 39 (2014) 8604–8608, https://doi.org/10.1016/J.IJHYDENE.2014.01.005.
[57] X. Zhu, Y. Shi, S. Li, N. Cai, Elevated Temperature Pressure Swing Adsorption Process for Reactive Separation of CO/CO 2 in H 2-Rich Gas, 2018, https://doi.org/10.1016/j.ijhydene.2018.05.030.
[58] X. Zhu, Y. Shi, S. Li, N. Cai, Two-Train Elevated-Temperature Pressure Swing Adsorption for High-Purity Hydrogen Production, 2018, https://doi.org/10.1016/j.apenergy.2018.08.093.
[59] R. Reijers, E. Van Selow, P. Cobden, J. Boon, R. Van Den Brink, SEWGS process cycle optimization, Energy Procedia 4 (2011) 1155–1161, https://doi.org/10.1016/j.egypro.2011.01.168.
[60] J. Boon, V. Spallina, Y. van Delft, M. van Sint Annaland, Comparison of the efficiency of carbon dioxide capture by sorption-enhanced water-gas shift and palladium-based membranes for power and hydrogen production, Int. J. Greenh. Gas Control. 50 (2016) 121–134, https://doi.org/10.1016/j.ijggc.2016.04.033.
[61] A.D. Wright, V. White, J.R. Hufton, R. Quinn, P.D. Cobden, E.R. Van Selow, Energy procedia CAESAR: development of a SEWGS model for IGCC, Energy Procedia 4 (2011) 1147–1154, https://doi.org/10.1016/j.egypro.2011.01.167.